RSC Advances

RSC Publishing

PAPER

View Article Online
View Journal | View Issue

Biofunctional magnetic nanotube probe for recognition and separation of specific bacteria from a mixed culture

Cite this: *RSC Advances*, 2013, **3**, 14634

Vinod Kumar,[a] Gopal Nath,[c] Ravinder. K. Kotnala,[d] Preeti S. Saxena*[a] and Anchal Srivastava*[b]

Received 10th May 2013,
Accepted 29th May 2013

DOI: 10.1039/c3ra42307g

www.rsc.org/advances

This study highlights the synthesis of an antibody conjugated magnetic carbon nanotube bioprobe for the recognition and separation of *Pseudomonas aeruginosa* (*P. aeruginosa*), a gram negative bacterium, from its mixed culture with *Staphylococcus aureus* (*S. aureus*). Multiwalled carbon nanotubes containing iron oxide nanoparticles (magnetic carbon nanotubes) were synthesized in a single step by a spray pyrolysis method. The synthesized magnetic nanotubes were characterized by X-ray diffraction, electron microscopy and magnetic property measurements. A *P. aeruginosa* specific rhodamine-labelled goat anti-*Pseudomonas* antibody was covalently attached to the magnetic carbon nanotubes to develop a bioprobe. Raman and Fourier transform spectroscopy studies were carried out to confirm the attachment of the antibodies to the magnetic nanotubes. The designed bioprobe was employed for the capture and subsequent separation of *P. aeruginosa* from its mixed culture with *S. aureus*. The probing efficiency of the developed bioprobe was characterized and confirmed by culturing the captured *P. aeruginosa* in selective media followed by fluorescence and scanning electron microscopy studies. A time dependent increase in the capture efficiency of the bioprobe for *P. aeruginosa* was noticed and found to be 65% within five minutes of incubation. Thus, the designed bioprobe presents a simple, reliable and cost effective diagnostic tool for rapid identification and separation of a particular bacterium from a site of co-infection which is of immense clinical relevance.

Introduction

Various pathogens that infect humans (*e.g.*, viruses, bacteria and fungal parasites) usually co-occur within human beings.[1] Instituting the nature and outcomes of co-infection requires integrated monitoring and research of different infectious diseases.[2] In the last few decades, the identification of pathogens in co-infections has developed into a strenuous issue in clinical research. For example, *Pseudomonas aeruginosa* (*P. aeruginosa*) and *Staphylococcus aureus* (*S. aureus*) are opportunistic pathogens and frequently co-infect the lungs of cystic fibrosis (CF) patients. The lack of pure microbiological information for the co-infection, leads to the prescription of sub optimal antibiotics.[3] Hence, the development of rapid and reliable methods for early and accurate identification as well as separation of the infectious microbes in a co-infection is very critical for the optimization of treatment with improved prognosis and reduced rate of mortality.

Conventional detection methods involve performing a combination of bacterial cultures, morphological investigations and assessment of biochemical/immunological parameters, which is time consuming and expensive with a dearth of reliability. A bioprobe is a tool or technique used for the qualitative and quantitative analysis of biomolecules, biological structures and microorganisms, and is promising for bioanalysis. In recent years, exclusive probes of magnetic nanoparticles have been developed and designed to identify and separate arrays of cells, pathogens and biomarkers.[4–7] Biofunctional magnetic nanoparticles have been reported for protein separation and detection of pathogens at ultra-low concentrations.[4,7] Difficulties in making monodispersed magnetic nanoparticles and robust chemistry for surface functionalization needs extra effort for the direct utilization of detection probes.

Carbon nanotubes, due to their unique physico-chemical properties, have stimulated considerable interest in various biological applications, particularly in the fields of biosensors (as a sensing platform),[8] vaccines and drug delivery (as vehicles).[9–11] The large surface area of carbon nanotubes,[9,11] with commendable surface bio-manipulation, makes them a suitable candidate to be used for the detection of pathogens.

[a]*Department of Zoology, Banaras Hindu University, Varanasi-221005, India. E-mail: pssaxena@rediffmail.com; Fax: 0542-2368174; Tel: 0542-2307149 (Ext-109)*
[b]*Department of Physics, Banaras Hindu University, Varanasi-221005, India. E-mail: anchalbhu@gmail.com; Fax: 0542-2368174; Tel: 0542-2307308 (O)*
[c]*Department of Microbiology, Institute of Medical Sciences, Banaras Hindu University, Varanasi-221005, India. E-mail: gopalnath@gmail.com*
[d]*National Physical Laboratory, New Delhi-110012, India. E-mail: rkkotnala@nplindia.org*

Galactosylated single walled carbon nanotubes[12] and immune-carbon nanotubes[13] have been reported so far, for capturing *Escherichia coli* in physiological solutions. The high surface area of carbon nanotubes may allow the attachment of a large number of biomolecules, and thus uphold the potential for ultrasensitive detection of pathogens. The introduction of ferromagnetism into carbon nanotubes has shown various interesting electronic and magnetic properties,[14–19] with further promise for bioanalysis.

In this study, we report a simple method for the single step synthesis of magnetic nanotubes, *i.e.* multiwalled carbon nanotubes containing iron oxide nanoparticles (Fe_2O_3@CNTs), for their further application in the development of a bioprobe (Ab–Fe_2O_3@CNTs) by attaching rhodamine-labelled goat anti-*Pseudomonas* antibodies to the nanotubes. The developed bioprobe was employed for the recognition and subsequent separation of *P. aeruginosa* (ATCC 27853) bacteria, from a mixed culture (considered as a model site of co-infection) with *S. aureus* (ATCC 25923).

Materials and methods

All the reagents used were of analytical grade. GFP-labelled *Pseudomonas aeruginosa* and a rhodamine-labelled goat anti-*Pseudomonas* antibody (Rh-anti-Psd-IgG) were purchased from Invitrogen Bio Services India Pvt. Ltd., Bangalore, India.

Synthesis of magnetic nanotubes (Fe_2O_3@CNTs)

Fe_2O_3@CNTs were synthesized by our previously developed spray pyrolysis method with slight modification.[20] In our earlier report, 2 mg ml^{-1} of xylene in ferrocene was the optimum condition for the growth of the nanotubes. In the present study, we have purposely taken a higher concentration of ferrocene in xylene (4 mg ml^{-1}) to obtain Fe_2O_3 nanoparticles encapsulated and decorated multiwalled carbon nanotubes (MWCNTs). In brief, a precursor solution of ferrocene in xylene with a concentration of 4 mg ml^{-1} was prepared. After putting the reaction chamber inside an electric furnace, the temperature was set to $\sim$950 °C. To create an oxygen free environment inside the chamber, it was flushed with argon gas. At 950 °C the ferrocene solution was fed at a constant flow rate of 2 ml min^{-1} in the form of a spray under steady flow of argon gas. The spraying was continued for 45 min, and during this time ferrocene and benzene dissociated and the deposition of Fe_2O_3@CNTs took place in the reaction chamber. To anneal the reaction products, the high temperature of the furnace was maintained for 15 min after the spraying ceased. The deposited Fe_2O_3@CNTs were collected and thoroughly washed with ethanol and distilled water.

Functionalization of magnetic nanotubes by amine ($-NH_2$) groups

The magnetic nanotubes were functionalized by amine groups employing a similar methodology reported earlier.[21,22] In brief, 100 mg of Fe_2O_3@CNTs were dispersed in a 100 ml mixture of H_2SO_4 and HNO_3 (3 : 1) by bath sonication {1 h at room temperature (RT)}. The suspension was filtered, dried and sonicated with 100 ml of HCl for 1 h to get carboxylated-magnetic nanotubes (–COOH–Fe_2O_3@CNTs), which were further filtered and vacuum dried (at 60 °C). Although most of the Fe_2O_3 nanoparticles present on the surface of the magnetic nanotubes dissolve during this process, the Fe_2O_3 present in the core and interstitial positions attribute to the magnetic properties. 25 mg of –COOH–Fe_2O_3@CNTs was dispersed in a 50 ml mixture of thionyl-chloride ($SOCl_2$) and dimethyl formamide (DMF) (20 : 1 v:v) at 70 °C for 24 h to obtain –$COCl_2$–Fe_2O_3@CNTs. The suspension of –$COCl_2$–Fe_2O_3@CNTs was filtered, washed with tetrahydrofuran (THF) and dried in vacuum (at RT). 50 ml of ethylenediamine (EDA) was added to 10 mg of –$COCl_2$–Fe_2O_3@CNTs and refluxed at RT for 12 h to get NH_2–Fe_2O_3@CNTs. The NH_2–Fe_2O_3–CNT suspension was filtered, washed with THF and dried under vacuum.

Attachment of the antibody to the magnetic nanotubes

Rh-anti-Psd-IgG was attached to –NH_2–Fe_2O_3@CNTs through an amide bond (–CO–NH–) formation between the –NH_2 group of –NH_2–Fe_2O_3@CNTs and the free –COOH group of the antibody. This was achieved by reacting 100 μl of (1 mg ml^{-1}) Rh-anti-Psd-IgG {(stock in 10 mM of 2-(*N*-morpholino) ethanesulfonic acid) (MES buffer)} to 5 ml of (1 mg ml^{-1}) –NH_2–Fe_2O_3@CNTs (pH 6.8) with slow agitation for 2 min. 1.2 mg of 1-ethyl-3-(3-dimethyl-aminopropyl) carbodiimide (EDC) was added to this mixture and allowed to react for 4 h at RT. Unbound antibodies were removed by centrifugation (at 4000 rpm for 15 min) and subsequent washing with MES buffer. The final product, as an antibody attached magnetic nanotube (Ab–Fe_2O_3@CNTs) bioprobe, was re-dispersed into MES buffer and stored at 4 °C for further application.

The developed bioprobe was further utilized for the identification and separation of *P. aeruginosa* bacteria from its mixed culture with *S. aureus* (details are given below).

Recognition and separation of *P. aeruginosa* from its pure culture

Although, the intention for developing the bioprobe was to identify and separate *P. aeruginosa* from a mixed culture, first the concentration dependent probing efficiency of the develop probe was optimized in a pure culture of *P. aeruginosa* (without *S. aureus*).

For this, a 200 μl suspension of 25, 50, 100 and 200 μg ml^{-1} of Ab–Fe_2O_3@CNTs was added to the culture of *P. aeruginosa* ($\sim 1 \times 10^6$ CFU ml^{-1}) and incubated for 5 min to facilitate the binding. The resulting Ab–Fe_2O_3@CNT–bacterial conjugates were separated by applying an external magnetic field (magnetic strength $\sim$400 G, Fig. 6bL). The capture efficiency of Ab–Fe_2O_3@CNTs was determined by the plate counting method. In brief, Ab–Fe_2O_3@CNT–bacterial conjugates were re-suspended into 50 μl of MES buffer and plated over a MH agar plate followed by overnight incubation at 37 °C. The supernatant was also plated and cultured in the same way as the Ab–Fe_2O_3@CNT–bacterial conjugates. The recovered bacteria were counted to determine the capture efficiency of Ab–Fe_2O_3@CNTs and the results were statistically analyzed by one-way ANOVA followed by *post hoc* Tukey's test using SPSS

software (version 12). The capture efficiency reported is the average of at least three replicates of the bacteria.

Recoginition and separation of *P. aeruginosa* from its mixed culture with *S. aureus*

S. aureus and *P. aeruginosa* were cultured separately to attain the maximum confluence of $\sim 5 \times 10^6$ CFU ml^{-1}. *S. aureus* and *P. aeruginosa* (each $\sim 1 \times 10^6$ CFU ml^{-1}) were mixed together in 5 ml of MES buffer. 5 different vials, each of which contained 5 ml mixed population of *S. aureus* and *P. aeruginosa* (each $\sim 1 \times 10^6$ CFU ml^{-1}), were used for the experiment. 200 μl (100 μg ml^{-1}, an optimized concentration in pure culture of *P. aeruginosa*) of Ab–Fe_2O_3@CNTs were added to each of the 5 vials, numbered as 1, 2, 3, 4, 5, containing the same number of mixed bacterial population, and were incubated for 5, 15, 30, 45 and 60 min respectively. An external magnet was applied on the wall of the vials after incubation to separate the captured *P. aeruginosa*, and the capture efficiency at the corresponding time interval was estimated by the plate counting method (as described above). The supernatant was also separated by gentle pipetting to estimate the capture efficiency. The results of the capture efficiency were statistically analyzed by one-way ANOVA followed by *post hoc* Tukey's test using SPSS software (version 12). The capture efficiency reported is the average of at least three replicates of the bacteria.

Characterization of probing efficiency of the Ab–Fe_2O_3@CNT bioprobe

The captured *P. aeruginosa* was identified by its growth on a cetrimide agar (a selective medium for *P. aeruginosa*). For this, the captured *P. aeruginosa* was diluted using sterile normal saline and plated on the cetrimide agar followed by incubation for 18 h at RT. However, the captured *P. aeruginosa* was also allowed to grow on a MHA agar to confirm the presence of contamination, if any. For this, the separated bacteria were cultured on a MHA agar for 18 h at RT. Further, scanning electron microscopy and fluorescence microscopy studies were carried out to confirm the binding of Ab–Fe_2O_3@CNTs to *P. aeruginosa*. For the SEM characterization, a sample of Ab–Fe_2O_3@CNT–bacterial aggregates was prepared with the following steps. In the first step, Ab–Fe_2O_3@CNT–bacterial aggregates were centrifuged at 5000 rpm followed by washing with MES buffer three times. In step two, the washed Ab–Fe_2O_3@CNT–bacterial aggregates were re-suspended in 0.25% of glutaraldehyde followed by overnight incubation (at RT). In step three, the suspension of the Ab–Fe_2O_3@CNT–bacterial aggregates was centrifuged at 5000 rpm and washed thrice with MES buffer. The fourth step is a dehydration step, where the Ab–Fe_2O_3@CNT–bacterial conjugates were subjected to an increasing concentration of ethanol, *i.e.* 30%, 50%, 70% and 90%, for 10 min each, and for 30 min in 100% ethanol. Finally, a drop of the suspension was taken over a SiO_2–Si substrate, dried at RT followed by gold coating, and SEM images were captured. Fluorescence microscope slides of Ab–Fe_2O_3@CNT–bacterial conjugates were prepared by pouring a thin film of conjugate over lysine pre-treated glass slides, and mounting under cover slip in Canada balsam. Observations were made using an appropriate filter.

Results and discussion

Synthesis and characterization of magnetic nanotubes (Fe_2O_3@CNTs)

The synthesis of Fe_2O_3@CNTs intended to combine the fundamental properties of both Fe_2O_3 and multiwalled carbon nanotubes (MWCNTs) for the development of a probe. The intentionally higher concentration of ferrocene used works as a catalyst for the synthesis of MWCNTs as well as a precursor for Fe_2O_3 nanoparticles. These Fe_2O_3 nanoparticles are responsible for introducing magnetic properties to the carbon nanotubes. The synthesized Fe_2O_3 nanoparticles sit on the surface and inner wall of MWCNTs to make the final structure, Fe_2O_3@CNTs. Fe_2O_3@CNTs were characterized by X-ray diffraction (XRD, Rigaku), transmission electron microscopy (FEI-Tecnai-20 UT, TEM), scanning electron microscopy (SEM LEO 440, SEM) and a physical property measurement system (QD-PPMS-6600) magnetometer.

In the XRD patterns of Fe_2O_3@CNTs (Fig. 1), the peak at 26.36° represents the characteristic peak of 002 reflection plane of MWCNT. The diffraction peaks corresponding to the peak positions match well the 220, 311, 511 and 440 reflection planes of Fe_2O_3 (PCPDF-07-0322, a = 8.390), confirming the synthesis of Fe_2O_3@CNTs. The magnetization curve of Fe_2O_3@CNTs (Fig. 2) shows the inter-relation between the extent of magnetization to the applied field at 300 K. The saturation in magnetization by Fe_2O_3@CNTs indicates that some Fe_2O_3 nanoparticles are in the super-paramagnetic state. Although pure carbon nanotubes exhibit diamagnetic properties,[23] the introduction of super-paramagnetism in Fe_2O_3@CNTs is due the presence of Fe_2O_3 nanoparticles. To get structural information about Fe_2O_3@CNTs, electron microscopic characterization was carried out. In the TEM micrograph (Fig. 3a), the decoration of MWCNTs by Fe_2O_3 nanoparticles can be seen in the red encircled areas, which was further confirmed through SEM investigations. The encapsulation and decoration of Fe_2O_3 nanoparticles (average size of 10 nm) on the surface of MWCNTs (average diameter of 80 nm) are more clearly visible in the SEM micrograph

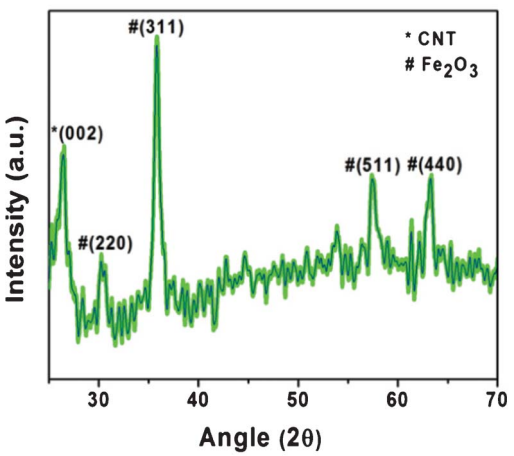

Fig. 1 Powder X-ray diffraction (XRD) pattern of Fe_2O_3@CNTs.

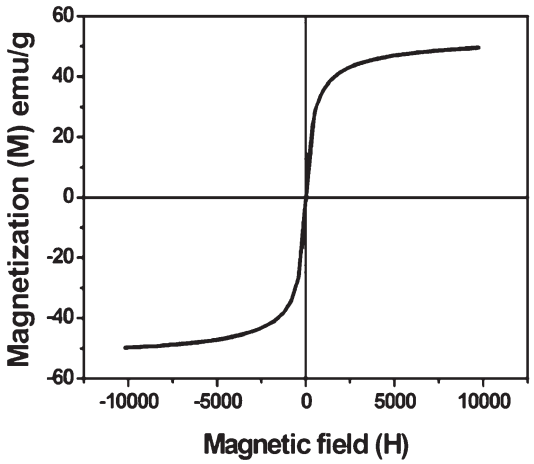

Fig. 2 Magnetization curve of Fe_2O_3@CNTs.

(Fig. 3b). The aggregates of Fe_2O_3 nanoparticles, which can be seen in the TEM image, are due to the inherent agglomeration properties of nanoparticles and the lack of a stabilizing agent. Energy dispersive X-ray spectroscopy (EDX) shown in Fig. 3c confirms the presence of the iron (Fe) and oxygen (O) atom in the magnetic nanotubes. TEM, SEM and EDX data further support the synthesis of Fe_2O_3@CNTs.

Characterization of antibody conjugation to magnetic nanotubes

Raman spectroscopy is a fast and non destructive tool for the characterization of carbon based nanomaterials. The Raman spectra of Fe_2O_3@CNTs, NH_2–Fe_2O_3@CNTs and Ab–Fe_2O_3@CNTs are shown in Fig. 4a.

In the Raman spectrum of Fe_2O_3@CNTs the D-band (disorder band) shows a peak value of 1351 cm^{-1} and the G-band (graphite) shows a peak at 1580 cm^{-1} with a 2D (second order harmonic) band at 2699 cm^{-1}. On $-NH_2$ functionalization a blue shift was observed in the D peak, *i.e.* a shift to 1348 cm^{-1}, which is more pronounced on attachment of the antibody, *i.e.* a shift to 1338 cm^{-1}, while both the G and 2D peaks almost remain constant in either

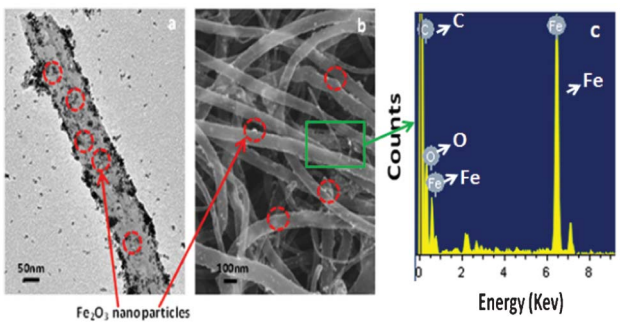

Fig. 3 Transmission electron micrograph (TEM) of (a) Fe_2O_3@CNTs, where encapsulation and decoration of Fe_2O_3 nanoparticles onto the MWCNTs can be seen, (b) scanning electron micrograph (SEM) of Fe_2O_3@CNTs, (c) EDX of Fe_2O_3@CNTs.

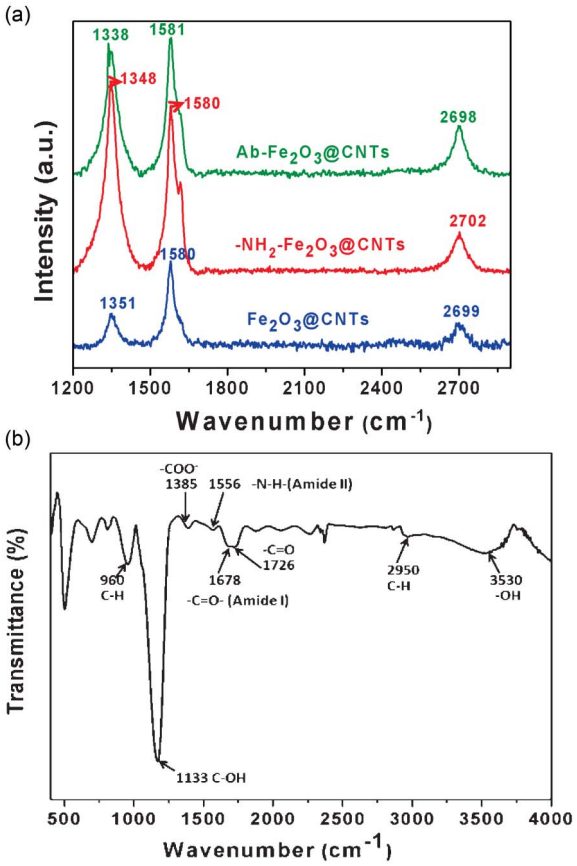

Fig. 4 (a) Raman spectra showing functionalization of magnetic nanotubes (Fe_2O_3@CNTs), (b) Fourier transform-infra red (FT-IR) spectra showing amide bond formation.

case. The process of functionalization was further supported by the intensity ratio I_D/I_G of the all three cases. In Fe@CNTs the value of I_D/I_G was 0.37 which increased to 1.10 on $-NH_2$ functionalization. On the other hand, upon the attachment of the antibody, I_D/I_G decreased to 0.94. The increase in I_D/I_G on $-NH_2$ functionalization may be attributed to the increased disorder in Fe@CNTs. However, the decrease in I_D/I_G on the addition of the antibody to NH_2–Fe@CNTs may be further attributed to the reduced disorder caused by the formation of an amide (–CO–NH–) bond between the $-NH_2$ free end of the functionalized magnetic nanotubes and the –COOH free end of the antibody.

FTIR results further verify the functionalization of Fe_2O_3@CNTs (Fig. 4b). The peak at 1385 cm^{-1} is due to –COO stretching, and represents the presence of the unmodified carboxylic acid group on the Fe_2O_3@CNT surface. The peaks at 1556 cm^{-1} and 3530 cm^{-1} represent the stretching of the –N–H– plane (amide II) and the vibration of the carbon skeleton of MWCNTs along with the peak of C=O– stretching (amide I) at 1678 cm^{-1}. The peaks showing amide I and amide II signatures confirm the attachment of the antibody to the NH_2–Fe_2O_3@CNTs. In addition, the peak at 1726 is due to the O–H bending vibration of the carboxyl group present on the surface of magnetic carbon nanotubes and the band observed

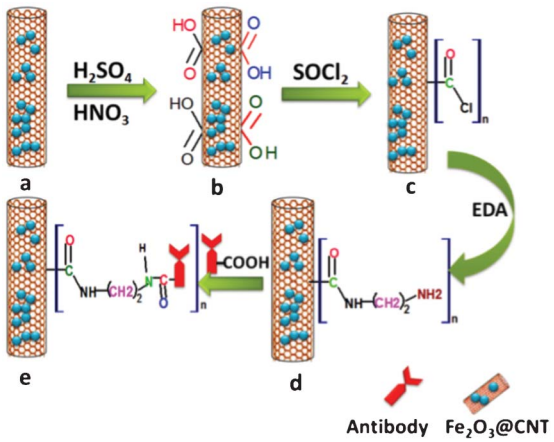

Fig. 5 Schematic diagram showing the functionalization of Fe_2O_3@CNT. (a) As synthesized Fe_2O_3@CNT, (b) –COOH group functionalized Fe_2O_3@CNT, (c) –$COCl_2$ functionalized Fe_2O_3@CNT, (d) –NH_2 functionalized Fe_2O_3@CNT, (e) Rh-anti-*Pseudomonas*-IgG antibody attached Fe_2O_3@CNTs (Ab–Fe_2O_3@CNTs).

at 1133 cm^{-1} is due to C–OH stretching vibrations. C–H stretching and bending vibrations are observed at 2950 cm^{-1} and 970 cm^{-1} respectively.

The different steps of the Fe_2O_3@CNT functionalization are shown with the help of a schematic diagram in Fig. 5.

Characterization (visual) of the magnetic properties of Fe_2O_3@CNTs and probing efficiency of Ab–Fe_2O_3@CNTs

The synthesis of Fe_2O_3@CNTs and probing efficiency of the developed Ab–Fe_2O_3@CNT bioprobe have been primarily characterized with the naked eye. A photograph (Fig. 6) showing the marked difference in the magnetic properties between the synthesized magnetic nanotubes (Fig. 6aL) and pure MWCNTs (Fig. 6aR taken as the control, under the magnetic field). Magnetic nanotubes possessing magnetic properties (due to the presence of Fe_2O_3 nanoparticles) were attracted under the influence of a magnetic field which is

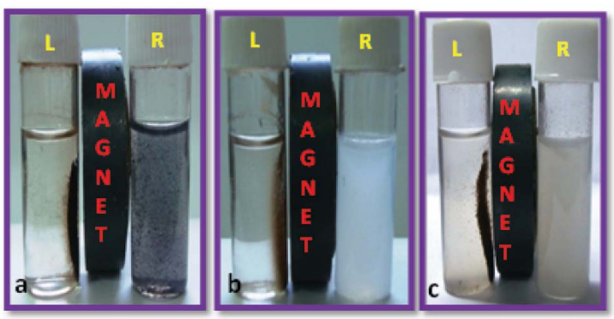

Fig. 6 Optical pictures of the identification and separation of *P. aeruginosa* bacteria from a mixed culture of *P. aeruginosa* and *S. aureus*. (a) Separated Fe_2O_3@CNTs (aL) and suspension of MWCNTs (aR) on application of an external magnet. (b) Separated *P. aeruginosa* with Ab–Fe_2O_3@CNTs (bL) and pure culture of *P. aeruginosa* without Ab–Fe_2O_3@CNTs (bR). (c) Separated *P. aeruginosa* with Ab–Fe_2O_3@CNTs from its mixed culture with *S. aureus* (cL) and mixed culture of *P. aeruginosa* and *S. aureus* (cR).

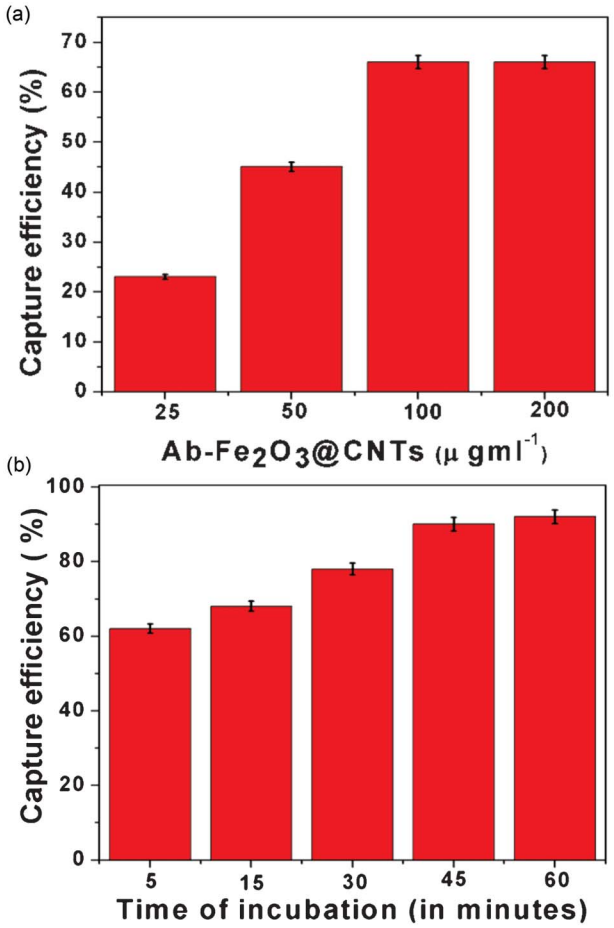

Fig. 7 (a) Capture efficiency with different concentrations of Ab–Fe_2O_3@CNTs. (b) Bar graphs representing the capture efficiency of Ab–Fe_2O_3@CNTs for *P. aeruginosa* as a function of time.

absent in the suspension of pure MWCNTs. In Fig. 6bL, the recognition and subsequent separation of *P. aeruginosa* from its pure culture can be seen, which is absent in the pure culture of *P. aeruginosa* (Fig. 6bR) without Ab–Fe_2O_3@CNTs. Fig. 6cL shows the identification and separation of *P. aeruginosa* by Ab–Fe_2O_3@CNTs from its mixed culture with *S. aureus*, which does not occur in Fig. 6cR without Ab–Fe_2O_3@CNTs.

Estimation of capture efficiency

Results of the concentration dependent optimization of capture efficiency (of Ab–Fe_2O_3@CNTs for *P. aeruginosa*) are shown in Fig. 7a. A concentration dependent increase in capture efficiency was observed up to 100 μg ml^{-1} Ab–Fe_2O_3@CNTs, therefore this was taken as the standard concentration for the estimation of time dependent capture efficiency. In the results shown in Fig. 7b, a time dependent increase in capture efficiency was observed. After five minutes of incubation it was found to be 65%, and reached 92% after 45 min of incubation (Fig. 7b). Conversely, in the supernatant, a decreased capture efficiency with time was found, which supports well the enhanced capture efficiency of Ab–Fe_2O_3@CNTs.

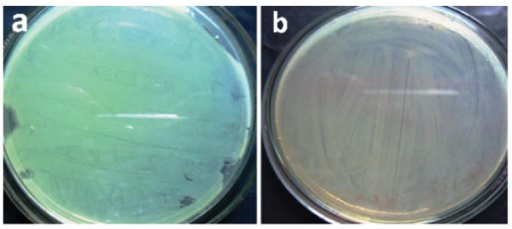

Fig. 8 Growth of separated *P. aeruginosa* on a MHA plate (a) and on a cetrimide agar (b).

Characterization of specificity of Ab–Fe_2O_3@CNTs

Growth of captured bacteria on a cetrimide agar, a selective medium for *P. aeruginosa*, confirms the specificity of the developed bioprobe (Fig. 8a). Further, a contamination free growth of the separated *P. aeruginosa* on the MH agar supports well the specificity of the bioprobe (Fig. 8b).

The specificity of the Ab–Fe_2O_3@CNT probe was further supported by a SEM study (Fig. 9), where the attachment of *P. aeruginosa* (from its mixed culture with *S. aureus*) to the bioprobe was observed, which can be seen more clearly in inset picture. Absence of *S. aureus* in the vicinity of *P. aeruginosa* in the SEM image (Fig. 9), further confirms the specificity of Ab–Fe_2O_3@CNTs. In order to doubly confirm the selectivity of the bioprobe for its target bacteria, fluorescence microscopy studies (Fig. 10) were carried out. The two white spots in the selected rectangular area of the phase contrast image (Fig. 10a) demonstrate the *P. aeruginosa* attached onto Ab–Fe_2O_3@CNTs, which is further visualized in the fluorescence images. The green fluorescent spots (at the place of white spots in the phase contrast image) in Fig. 10b are due to the green fluorescent protein, which is conjugated to *P. aeruginosa*, and denote the presence of *P. aeruginosa*. The red fluorescent spots (Fig. 10c) at the place of the green fluorescent spots (Fig. 10b) are due to rhodamine conjugated to the anti-*Pseudomonas* antibody (Rh-anti-Psd-IgG) functionalized over magnetic nanotubes, providing an indication regarding the presence of magnetic nanotubes. The red spots exactly at the place of the green spots reveal the specific binding of *P. aeruginosa* to the Ab–Fe_2O_3@CNTs. A merged image (Fig. 10d) of Fig. 10b and Fig. 10c shows the co-localization of green and red signals, doubly confirming the binding of *P. aeruginosa* to Ab–Fe_2O_3@CNTs. A schematic representation of the specific recognition and separation of *P. aeruginosa* (from its mixed culture with *S. aureus*) is illustrated in Fig. 11.

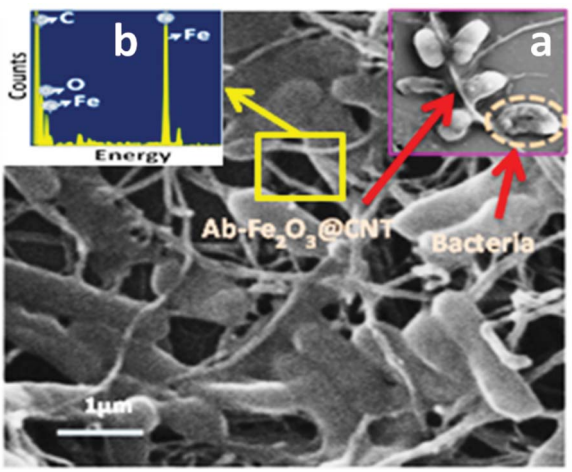

Fig. 9 Scanning electron micrograph (SEM) of the attachment of *P. aeruginosa* on Ab–Fe_2O_3@CNTs, which is more clear in the inset picture.

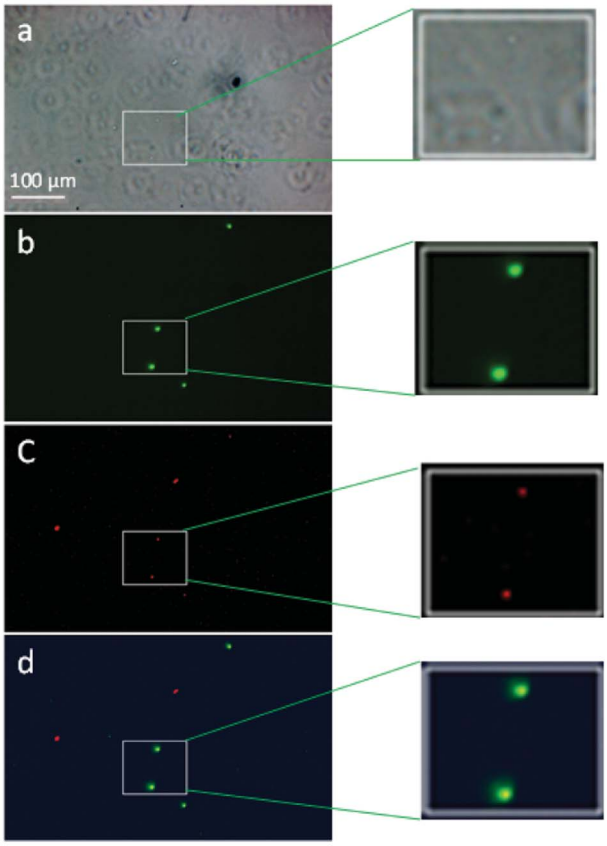

Fig. 10 (a) Phase contrast image showing the attachment of *P. aeruginosa* to the Ab–Fe_2O_3@CNTs. (b) Green fluorescence (inside rectangular box) shows the presence of GFP labelled *P. aeruginosa* attached to the Ab–Fe_2O_3@CNTs. (c) Red fluorescence is due to Rh-anti-Psd-IgG attached to Fe_2O_3@CNTs. (d) Merged images of (b) and (c) showing the co-localization of red and green fluorescence, thus confirms the attachment of *P. aeruginosa* to the Ab–Fe_2O_3@CNTs. The squares in front of each figure show the zoomed-in image of the selected rectangular area.

Bacterial surface charge, hydrophobicity and other surface properties have a great impact on the capture efficiency.[16] The enhanced capture efficiency of Ab–Fe_2O_3@CNTs is primarily attributed to the specific binding between major cell-wall lipopolysaccharide antigens, *O*-antigen of *P. aeruginosa*, to the complementary antibody at Ab–Fe_2O_3@CNTs. The large surface area of the Ab–Fe_2O_3@CNT probe allows the binding of a maximum number of bacterial cells with time, playing a significant role towards enhanced capture efficiency.

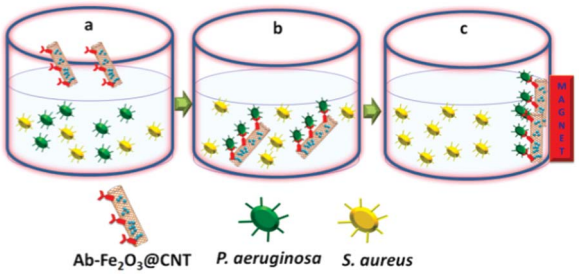

Fig. 11 Schematic diagram showing the attachment onto Ab–Fe_2O_3@CNTs and separation of *P. aeruginosa* from its mixed culture with *S. aureus*. (a) Introduction of Ab–Fe_2O_3@CNTs into the mixed culture of *P. aeruginosa* and *S. aureus*. (b) Specific attachment of Ab–Fe_2O_3@CNTs to *P. aeruginosa* and not *S. aureus*. (c) Separation and subsequent deposition of *P. aeruginosa* on Ab–Fe_2O_3@CNTs on the side wall of the pot on application of an external magnet.

Earlier, several efforts have been made for the detection and separation of pathogens, most of them employing iron nanoparticles with different surface functionalization, *e.g.* biofunctionalization by vancomycin[4,7,24,25] and carbohydrate molecules.[26,27] Vancomycin functionalized iron nanoparticles allow the detection of both gram positive and gram negative bacteria even at a very low concentration, but lack of specificity of the detection system is the major concern. However, Ab–Fe_2O_3@CNTs show a high specificity due to the high affinity between antigen and antibody (Fig. 4, 7–10), which is the primary and utmost requirement for any detection system.

Employing the magnetic relaxation technique, tailored magnetic nanoparticles have been used for the specific detection of *Brucella*, a deadly pathogen.[28] The complex and uncommon nature of the detection technique (magnetic relaxation) further limits its general applicability. On the other hand, a microscopy enabled detection system for Ab–Fe_2O_3@CNTs is very common and used routinely, making it a useful detection tool. Considering the electrostatic attraction between the amine group and negatively charged bacterial surface, amine functionalized magnetic nanoparticles have been applied for rapid capture and removal of bacterial pathogens.[29] Although the reported technique is very simple, specificity is again a matter of consideration. Silica-encapsulated super-paramagnetic nanoparticles have been investigated for the specific capturing of polystyrene beads (a model for bacteria).[30] Polystyrene beads can mimic the shape and size of bacteria, but fail to mimic the surface structure and properties which play an important role in specific binding. Conversely, Ab–Fe_2O_3@CNTs bind specifically to the cell surface antigen of the bacteria, thus avoiding ambiguity in the results. The architecture and orientation of vancomycin, attached to iron nanoparticles, affects the capture efficiency for polystyrene beads (modified by vancomycin antibody).[31] However, analysis of biological samples is obscure, which is highly concerning for its general practicability.

The results of our present study show that Ab–Fe_2O_3@CNTs possess an excellent recognition as well as separation ability of a particular pathogen from a mixed culture (a model site of co-infection), which can have a strong impact in clinical applications where optimization of therapy takes a long time and sometimes leads to fatal results due to co-infection. To the best of our knowledge this is first study which delivers insight to the recognition and subsequent separation of individual bacteria from a mixed culture using the Ab–Fe_2O_3@CNT probe. The high capture efficiency of the developed Ab–Fe_2O_3@CNT probe imparts its further suitability for applications where ultrasensitive probes for pathogen capturing are desired.

Conclusions

In summary, we have demonstrated the synthesis of an antibody conjugated magnetic nanotube (Ab–Fe_2O_3@CNT) bioprobe by the incorporation of magnetic nanoparticles onto multiwalled carbon nanotubes and their subsequent functionalization with the Rh-anti-*Pseudomonas*-IgG antibody. A single step synthesis of magnetic nanotubes using a spray pyrolysis method (with slight modification) is reported. The magnetic nanotubes were characterized by XRD, TEM, SEM and PPMS techniques. A *P. aerugionsa* specific antibody was attached to the magnetic nanotubes in order to develop a bioprobe. The developed bioprobe was employed for the selective binding and separation of *P. aeruginosa* bacteria from its mixed culture with *S. aureus*. A specific and rapid response towards the recognition and separation of *P. aeruginosa* was displayed by the bioprobe. Identification of the captured and separated *P. aeruginosa* was confirmed by its growth on selective media (cetrimide agar), which was further supported by SEM and fluorescence microscopic studies. On estimating the capture efficiency, it was noticed that the bioprobe not only detects *P. aeruginosa* in less than a minute, but removes up to 65% of the target bacteria from its mixed culture in just 5 min. The high surface area with magnetic properties of the developed Ab–Fe_2O_3@CNT bioprobe presents a simple and reliable bio-analytical tool for the recognition and separation of a particular pathogen in a co-infection, which is a rapid and cost effective approach. Further research is needed to explore the utilisation of the Ab–Fe_2O_3@CNT bioprobe in biological samples, wherein co-infection is caused by bacteria–bacteria, bacteria–fungi, or bacteria–virus.

Acknowledgements

V. K. acknowledges UGC, New Delhi, India, for providing financial support as RGNF, Dr C. Upadhyay, School of Material Science and Technology, IIT, BHU, India, for helping in the SEM characterization, Prof. S. C. Lakhotiya and Mr. Anand Singh for fluorescence microscopy. V. K. also acknowledges Deep Jariwala, Northwestern University, USA, N.R Nirala, B.H.U., India, for their valuable suggestions and help towards the manuscript preparation. P. S. Saxena acknowledges the CAS program in the Zoology Department, B.H.U., Varanasi, India, funded by UGC. A. Srivastava acknowledges the DST, New Delhi, India, and CAS Department of Physics, Banaras Hindu University, India.

References

1 K. A. Brogden, J. M. Guthmiller and C. E. Taylor, *Lancet*, 2005, **365**, 253–255.
2 P. Steinmann, J. Utzinger, Z.-W. Du and X.-N. Zhou, *Adv. Parasitol.*, 2010, **73**, 21–50.
3 Y.-C. Lin, C.-Y. Tu, W. Chen, Y.-L. Tsai, H.-J. Chen, W.-H. Hsu and C.-M. Shih, *Intern. Med.*, 2007, **46**, 1173–8.
4 H. Gu, K. Xu, C. Xu and B. Xu, *Chem. Commun.*, 2006, 941–9.
5 K.-C. Ho, P.-J. Tsai, Y.-S. Lin and Y.-C. Chen, *Anal. Chem.*, 2004, **76**, 7162–8.
6 P.-C. Lin, P.-H. Chou, S.-H. Chen, H.-K. Liao, K.-Y. Wang, Y.-J. Chen and C.-C. Lin, *Small*, 2006, **2**, 485–9.
7 H. Gu, P.-L. Ho, K. W. T. Tsang, L. Wang and B. Xu, *J. Am. Chem. Soc.*, 2003, **125**, 15702–3.
8 D. Jariwala, V. K. Sangwan, L. J. Lauhon, T. J. Marks and M. C. Hersam, *Chem. Soc. Rev.*, 2013, **42**, 2824–2860.
9 Y. Lin, S. Taylor, H. Li, K. A. S. Fernando, L. Qu, W. Wang, L. Gu, B. Zhou and Y.-P. Sun, *J. Mater. Chem.*, 2004, **14**, 527.
10 P. M. Ajayan, *Chem. Rev.*, 1999, **99**, 1787–1800.
11 N. W. Shi Kam, T. C. Jessop, P. A. Wender and H. Dai, *J. Am. Chem. Soc.*, 2004, **126**, 6850–1.
12 T. Elkin, X. Jiang, S. Taylor, Y. Lin, L. Gu, H. Yang, J. Brown, S. Collins and Y.-P. Sun, *ChemBioChem*, 2005, **6**, 640–3.
13 L. Gu, T. Elkin, X. Jiang, H. Li, Y. Lin, L. Qu, T.-R. J. Tzeng, R. Joseph and Y.-P. Sun, *Chem. Commun.*, 2005, 874–6.
14 Y. Li, T. Kaneko, T. Ogawa, M. Takahashi and R. Hatakeyama, *Chem. Commun.*, 2007, 254–6.
15 S. Pal, S. Chandra, M.-H. Phan, P. Mukherjee and H. Srikanth, *Nanotechnology*, 2009, **20**, 485604.
16 Y. Krupskaya, C. Mahn, A. Parameswaran, A. Taylor, K. Krämer, S. Hampel, A. Leonhardt, M. Ritschel, B. Büchner and R. Klingeler, *J. Magn. Magn. Mater.*, 2009, **321**, 4067–4071.
17 O. Vittorio, P. Quaranta, V. Raffa, N. Funel, D. Campani, S. Pelliccioni, B. Longoni, F. Mosca, A. Pietrabissa and A. Cuschieri, *Nanomedicine*, 2011, **6**, 43–54.
18 U. Weissker, S. Hampel, A. Leonhardt and B. Büchner, *Materials*, 2010, **3**, 4387–4427.
19 S. Kopyl, V. Bystrov, I. Bdikin, M. Maiorov and A. C. M. Sousa, *J. Mater. Chem. C*, 2013, **1**, 2860.
20 A. Srivastava, O. N. Srivastava, S. Talapatra, R. Vajtai and P. M. Ajayan, *Nat. Mater.*, 2004, **3**, 610–4.
21 J. Chen, A. M. Rao, S. Lyuksyutov, M. E. Itkis, M. A. Hamon, H. Hu, R. W. Cohn, P. C. Eklund, D. T. Colbert, R. E. Smalley and R. C. Haddon, *J. Phys. Chem. B*, 2001, **105**, 2525–2528.
22 Y. Chen, R. C. Haddon, S. Fang, A. M. Rao, P. C. Eklund, W. H. Lee, E. C. Dickey, E. A. Grulke, J. C. Pendergrass, A. Chavan, B. E. Haley and R. E. Smalley, *J. Mater. Res.*, 1998, **13**, 2423–2431.
23 K. Lafdi, A. Chin, N. Ali and J. F. Despres, *J. Appl. Phys.*, 1996, **79**, 6007.
24 H. Gu, P.-L. Ho, K. W. T. Tsang, C.-W. Yu and B. Xu, *Chem. Commun.*, 2003, 1966.
25 J. Gao, L. Li, P.-L. Ho, G. C. Mak, H. Gu and B. Xu, *Adv. Mater.*, 2006, **18**, 3145–3148.
26 K. El-Boubbou, C. Gruden and X. Huang, *J. Am. Chem. Soc.*, 2007, **129**, 13392–3.
27 C.-C. Lin, Y.-C. Yeh, C.-Y. Yang, C.-L. Chen, G.-F. Chen, C.-C. Chen and Y.-C. Wu, *J. Am. Chem. Soc.*, 2002, **124**, 3508–3509.
28 A. Fornara, P. Johansson, K. Petersson, S. Gustafsson, J. Qin, E. Olsson, D. Ilver, A. Krozer, M. Muhammed and C. Johansson, *Nano Lett.*, 2008, **8**, 3423–8.
29 Y.-F. Huang, Y.-F. Wang and X.-P. Yan, *Environ. Sci. Technol.*, 2010, **44**, 7908–13.
30 A. J. Kell, K. Somaskandan, G. Stewart, M. G. Bergeron and B. Simard, *Langmuir*, 2008, **24**, 3493–502.
31 A. J. Kell and B. Simard, *Chem. Commun.*, 2007, 1227–9.